Ceramics-Silikáty 66 (2), 178-187 (2022)
www.ceramics-silikaty.cz 10.13168/cs.2022.0012

CHLORIDE DIFFUSION IN CORAL AGGREGATE CONCRETE EXPOSED TO DIFFERENT MARINE CORROSION ENVIRONMENTS

#DAGUAN HUANG *, DITAO NIU**, YUNHE LIU*, LI SU***,QIAN XIA*, BINGBING GUO**

*School of Civil Engineering and Architecture, Xi'an University of Technology, Xi'an 710048, China
**College of Civil Engineering, Xi'an University of Architecture & Technology, Xi'an 710055, China
***School of Civil Engineering, Lanzhou University of Technology, Lanzhou 730050, China

#E-mail: hdg0505@163.com

Submitted December 23, 2021; accepted February 21, 2022

Keywords: Coral aggregate concrete, Submerged zone, Tidal zone, Salt spray zone, Chloride transport

In this paper, the chloride diffusion behaviour of coral aggregate concrete (CAC) exposed to marine submerged, tidal, and salt spray zones was investigated, and the effect of the fly ash (FA) content on the chloride diffusion was explored. The chloride concentration was measured using the potentiometric method, and the $Ca(OH)_2$ content in the CAC was calculated using the thermogravimetric method. The results show that the chloride concentration in the submerged zone decreases with an increasing erosion depth; meanwhile, in the tidal and salt spray zones, the chloride concentration showed a two-stage distribution pattern. The depth of the convective zone gradually increases with an increasing erosion time, and the depth of the convective zone in the salt spray zone is larger than that in the tidal zone. The chloride diffusion coefficient exhibits a power-function attenuation relationship with erosion time when exposed to different corrosion zones. The attenuation coefficient of the chloride diffusion coefficient increases with an increasing FA content. Moreover, the attenuation coefficient is the highest in the salt spray zone with it being 10.8 % to 28.5 % higher than that of the tidal zone. In addition, the $Ca(OH)_2$ content in the tidal zone is not only the lowest, but also gradually decreases with an increasing erosion time.

INTRODUCTION

As a society develops, land resources are continuously consumed, and countries all over the world have turned their strategic attention to the seas with their rich resources. All countries are vigorously promoting the construction of island infrastructures to improve the development capacity of marine resources. Large amounts of concrete materials are needed for the construction of island projects [1]. Coarse and fine aggregates make up more than 70 % of the total volume of concrete and are in high demand for island construction [2]. However, there is not enough conventional gravel and river sand to make the concrete on the islands. If all the raw materials are transported from the mainland, the cost of large-scale infrastructure construction will increase sharply, and the construction period cannot be guaranteed, which restricts the development and construction of islands and reefs to a great extent. To accelerate the construction of marine islands and reefs, alternative materials to conventional aggregates are urgently required. Relevant studies have found that the main structures of marine islands are coral reefs. A coral reef is a special rock body developed in tropical marine environment and formed by the skeletons of the coral groups after death. Its chemical composition is mainly calcium carbonate, which can provide rich new building materials for the construction of marine islands [3-5]. Research on coral aggregate concrete (CAC) began early in the United States. After World War II, roads, airports, and other structures were built on islands in the Western Pacific (Midway Island and Saipan Island) [6]. Research on coral aggregates in China started later; and following the rapid increase in island projects, such research is increasing [7]. Therefore, for offshore islands, coral gravel on the island can be used as an aggregate to prepare the CAC; this can effectively reduce the construction costs of island reef engineering and accelerate construction processes, which is of great significance to the marine economic development.

In recent years, the development of and research into coral aggregates has received considerable attention. Coral sand and gravel aggregates can be used to prepare concrete, which can solve the material shortage and accelerate a project's construction. However, waste coral reef sand is often used to reduce the environmental load [8]. Initially, researchers mainly discussed the basic mechanical properties of CAC. The strength grade of the CAC was less than C30 in the early stages, though it was improved during later stages. Marine areas feature high humidity, high salinity, and have prominent durability problems [9, 10]. Therefore, the gap between the durability of CAC and ordinary aggregate concrete has become an important factor restricting the development and construction of islands. The chloride present in marine environments is an important factor affecting the durability of concrete. Therefore, the primary task was to study the chloride corrosion resistance of CAC. Several practical engineering field tests showed that the chloride corrosion resistance of CAC is poorer than that of ordinary concrete [11, 12]. Yu et al. showed that, under identical environmental conditions, the surface chloride concentration of CAC was 13–28 times that of ordinary aggregate concrete [13]. Dou et al. and Huang et al. studied the anti-chloride corrosion behaviour of CAC, by simulating the submerged zone of a marine environment in the laboratory [14, 15]. The results showed that the chloride concentration and growth rate in CAC exceeds those in ordinary aggregate concrete, and the surface chloride concentration exhibits a power function increase with respect to the erosion time. Owing to the different service environments of concrete structures, the chloride penetration into the concrete may differ. To our knowledge, no comparative analysis of the chloride diffusion in CAC exposed to different erosion zones has been performed. Therefore, systematic research on the chloride diffusion behaviour of CAC in marine submerged, tidal and salt spray areas is needed.

Environmental pollution and energy consumption are important global problems. Research shows that the quantity of cement in CAC exceeds that in ordinary concrete. According to the relevant data, each tonne of cement production consumes large amounts of other fuels and emits 0.8–1.2 tonnes of carbon dioxide into the atmosphere [16]. Fly ash (FA) is a by-product of modern coal-fired power plants. Following the development of the power industry, FA production has also increased every year. If not reasonably disposed of, this will not only cause soil and air pollution, but also endanger human health and the ecology. Relevant studies have shown that the activity and micro-aggregate effects of FA can improve the performance of concrete. Therefore, replacing a percentage of the cement in CAC with FA not only reduces the cement consumption and saves energy, but also solves the environmental pollution problems of FA [17, 18]. The research shows that the addition of FA to CAC can effectively reduce the latter's chloride diffusion coefficient; however, simply adding more FA is not ideal [19, 20]. Therefore, it is necessary to further investigate the optimal amount of FA.

According to the aforementioned studies, few comparative analyses of chloride ingress have been reported for CAC under different erosion environments. Therefore, this study aims to identify the laws of chloride diffusion in CAC in different marine corrosion zones and analyse the influence of the FA content on the chloride diffusion performance of CAC exposed to different corrosion zones. Then, the micro-test method was used to identify the chloride erosion mechanism. The research results can provide a theoretical basis for the durability design of CAC in different service environments.

EXPERIMENTAL

Raw materials

The cementitious materials used in the preparation of CAC include P.O 42.5R ordinary Portland cement and fly ash (FA). The physical properties and chemical compositions of the cementitious materials are summarised in Table 1. The coarse aggregate (CA) had particle sizes ranging from 5 to 20 mm; the fine aggregate (S) had a fineness modulus of 2.8. Local tap water supplied to Xi'an was used as the water (W) for mixing and curing. A polycarboxylate high-performance water-reducing agent was used; it had a water-reducing rate of 30 %.

Table 1. Chemical composition of the cementitious materials.

Item	SiO_2 (%)	Al_2O_3 (%)	Fe_2O_3 (%)	CaO (%)	MgO (%)	SO_3 (%)	K_2O (%)	Density ($g \cdot cm^{-3}$)
OPC	21.18	5.02	3.14	63.42	3.12	2.30	0.65	3.10
FA	35.71	16.57	8.92	21.14	1.41	1.94	0.80	2.35

The coral aggregate was the original coral salvaged from an island in Xisha, the South China Sea, as shown in Figure 1. The surface of this coral aggregate is porous, and its microstructure is shown in Figure 2. According to the gradation requirements of ordinary aggregate crushing, the coral aggregate was divided into coarse and fine categories. The grading curve and physical properties of the coral aggregate can be found in Reference 2 and Reference 15, respectively.

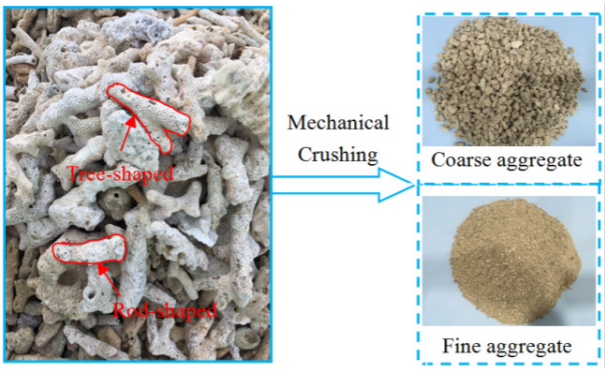

Figure 1. Coral aggregate.

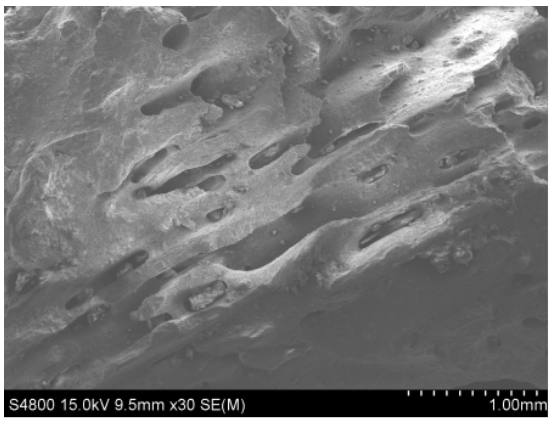

Figure 2. SEM of the coral aggregate.

Mix proportions

The mix proportions of the concrete are listed in Table 2. In this study, C30F15 represents CAC with a strength grade of C30 and an FA content of 15 %. The mix proportions of other CACs can be understood using these examples.

Testing methods

Chloride erosion test

Concrete cube specimens (side length: 100 mm) were used for the tests. All the specimens were cured for 28 days (d) under standard curing conditions of 20 ± 2 °C and 98 % humidity. The natural soaking method was adopted in the submerged zone, as shown in Figure 3 (a). The tidal zone was simulated by a dry-wet cycle, as shown in Figure 3 (b). First, the specimen was immersed in the erosion solution for 24 h before being removed from there and then dried in an air-blast drying oven at 50 °C for 24 h, with a dry-wet cycle of 48 h. A salt spray test chamber was used to conduct the tests in the salt spray zone, as shown in Figure 3 (c). A YWX / Q-020 salt spray corrosion test chamber (Wuxi Sunan Experimental Equipment Co., Ltd.) was used in the test. The intermittent spraying mode was adopted (i.e., spraying for 12 h and intermittent for 12 h). The test solution was a 3.5 % NaCl solution, the temperature was 35 ± 2 °C, and the salt spray sedimentation rate was 1–2 mL /80 (cm^2·h). The test was divided into five cycles: 30, 60, 90, 120, and 180 d of erosion.

Table 2. Mix proportions ($kg·m^{-3}$).

Specimen	PC	CA	Sand	Water	FA	PBS
C30F0	525	600	900	183.75	-	5.25
C30F15	446.25	600	900	183.75	78.75	5.25
C30F30	367.5	600	900	183.75	157.5	5.25
C30F45	288.75	600	900	183.75	236.25	5.25

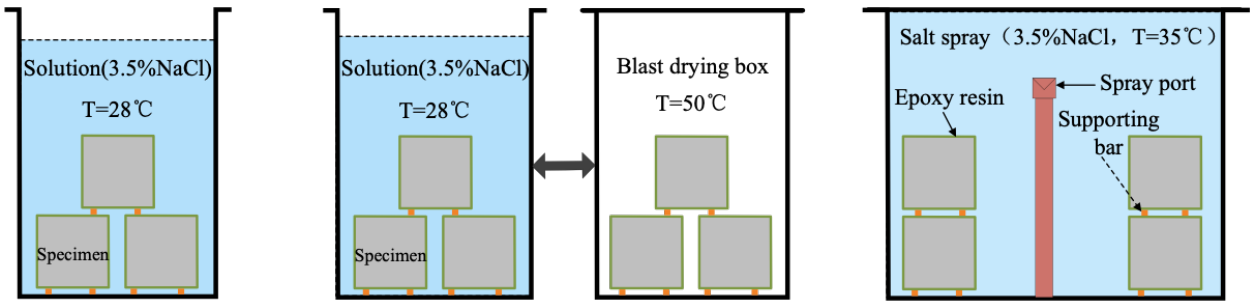

(a) Submerged zone (b) Tidal zone (c) Salt spray zone

Figure 3. Schematic diagram of the erosion tests.

Free chloride test

The free chloride concentration in the CAC was measured by referring to the potentiometric method in "Testing code of concrete for port and waterwog engineering", as shown in Figure 4. After the end of each erosion time, powder was taken for use. Before the test, the sample powder was dried in a vacuum drying box at 50 °C for 1 day to remove the water, then 5 g of powder was weighed and soaked in 100 mL of distilled water. After oscillation on an oscillator for 5 min, the filtrate was taken for the test after standing for 1 day. The equation:

$$W_{[Cl^-]}\% = \left(\frac{M_{[Cl^-]} \times 10^{-P[Cl^-]} \times V}{G} \right) \times 100\% \quad (1)$$

was used for the calculation, where $W_{[Cl^-]}\%$ is the percentage of the free chloride ions in the hardened concrete relative to the mass of concrete powder (%), $M_{[Cl^-]}\%$ is the molar mass of the chloride ions (35.45 $g \cdot mol^{-1}$), and G is the mass of the concrete powder used for soaking (g). V is the volume of the soaking solution (mL).

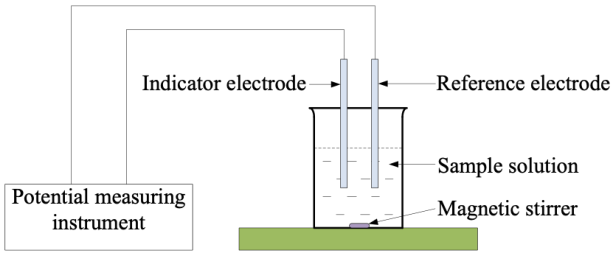

Figure 4. Schematic diagram of the potentiometric test.

Microscopic analysis

Microscopic tests included X-ray diffraction (XRD) and a thermogravimetric analysis (TGA). The concrete samples were continuously scanned from 5° to 35°. The TGA was performed using a simultaneous thermal analyser in a nitrogen atmosphere.

EXPERIMENTAL RESULTS AND DISCUSSIONS

Chloride concentration distribution

Distribution law of the chloride concentration

The chloride concentration distributions in the concrete exposed to the different erosion zones are shown in Figure 5. In the different erosion zones, the chloride concentration gradually increased with an increase in the erosion time; however, the increase amplitude gradually decreased. In the submerged zone, the chloride concentration gradually decreased with an increasing erosion depth and finally stabilised at some distance from the surface of the CAC. The reduction rate was large in the early stage and small in the later stages. In the tidal and salt spray zones, the chloride concentration curve can be separated into two sections: ascending and descending sections. The ascending section corresponded to the capillary adsorption area, and the descending one corresponded to the diffusion area. As can be seen from Figure 5, with the increase in the FA content, the chloride concentration in the CAC first decreased and then increased; a similar trend was observed in terms of the depth at which the chloride concentration stabilised, because the FA addition to the concrete improves its workability, increases its viscosity, and refines its pore structure. The harmful pore content in the CAC was reduced, and the resistance to chloride diffusion was increased. In addition, the secondary hydration product of FA reacted with free chloride to form Friedel's salt, which also reduced the chloride concentration in the pore solution [21]. However, when the FA content exceeded the optimum value, the micro-aggregate effect decreased, the number of harmful pores increased, the diffusion resistance of the chloride decreased, the content of the chloride increased, and the depth at which the chloride reached a stable stage also increased.

Depth of convection zone

From the above analysis, it can be seen that, in contrast to the monotonic attenuation (with respect to erosion depth) of chloride concentration in the submerged zone, the peak chloride concentration of the CAC in the tidal zone and salt spray zone appears at a certain depth inside the concrete. At present, scholars at home and abroad typically refer to the distance between the concrete surface and erosion depth of the peak concentration as the convection zone. The formation of a chloride convection zone in concrete is closely related to its internal pore structure. The concrete features a pore microstructure similar to an "inkbottle-beam tube" [22]. In the wetting state, the external solution penetrated into the concrete under the combined action of capillary adsorption and the concentration gradient, and the external chloride ions invaded the concrete, as shown in Figure 6a. The pore liquid inside the concrete migrated outward via surface evaporation, and the evaporation of the pore liquid from the concrete surface was rapid. Because the connecting holes were blocked, the evaporation rate of the internal pore liquid was very slow, and a delayed lag effect was observed. The chloride ions in the surface layer accumulated, owing to the rapid evaporation of the pore liquid; as a result, the concentration increased at a certain depth from the surface layer. Meanwhile, the change

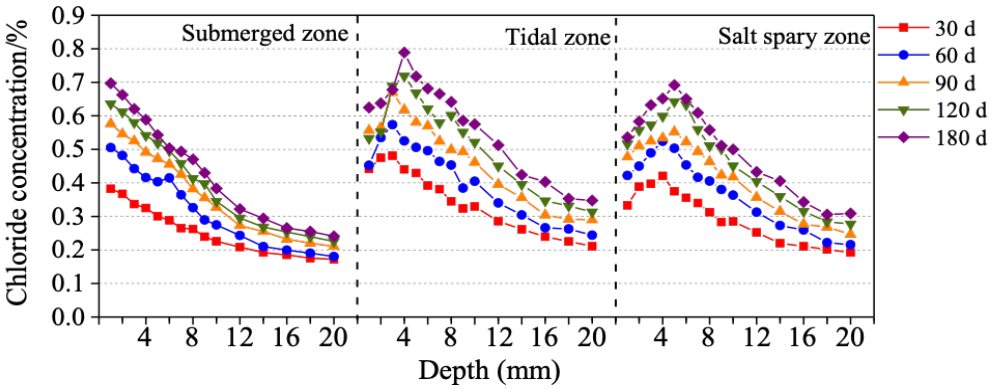

(a) C30F0

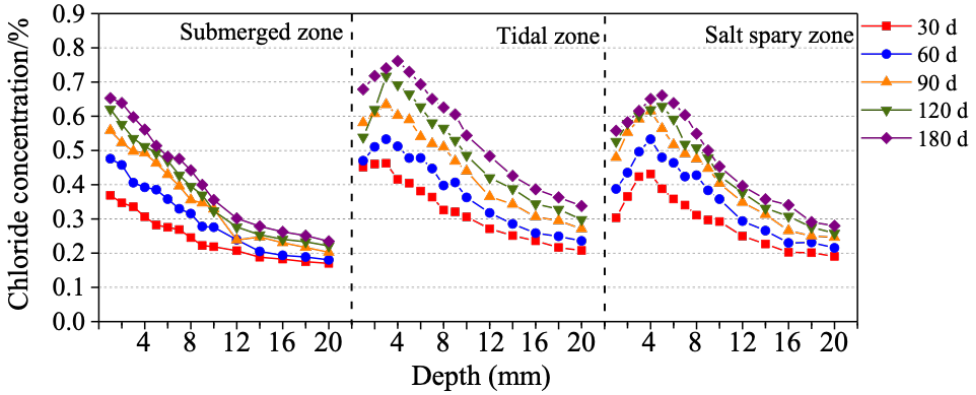

(b) C30F15

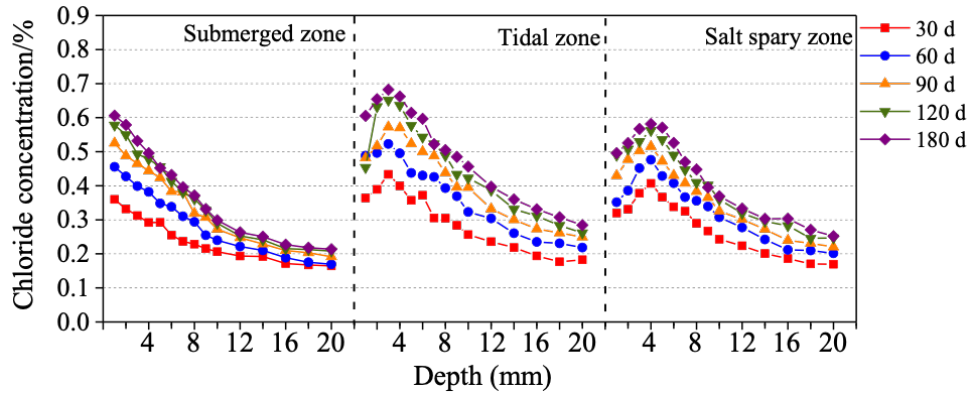

(c) C30F30

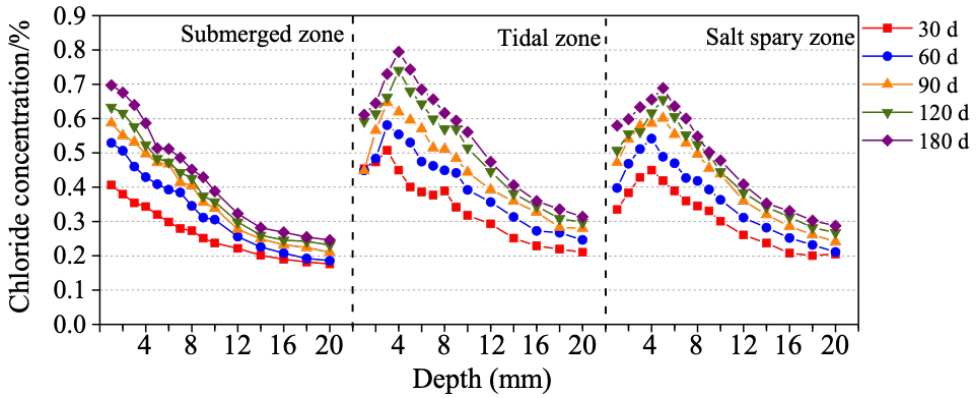

(d) C30F45

Figure 5. Chloride concentration curves of the concrete in the different corrosion zones.

in the pore liquid saturation with respect to concrete depth was very small. When the concrete was wet again, the high dryness of the surface concrete meant that the chloride ions rapidly penetrated the concrete via the pore fluid, and the pore fluid of the surface concrete was rapidly supplemented. Meanwhile, the ion concentration at the surface may have exceeded that of the external solution, causing diffusion to the surface; however, the intensity of the convection was greater than that of the diffusion, and the chloride ions were continuously transmitted into the concrete. Therefore, under the repeated action of drying and wetting, the concentration peak appeared at a certain depth from the concrete surface.

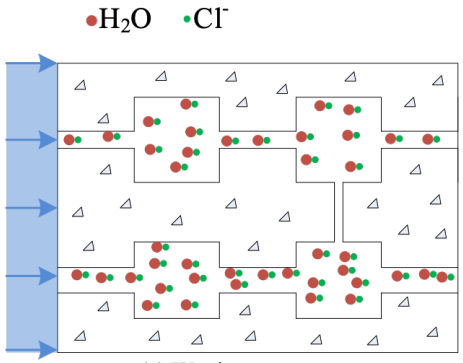

(a) Wetting state

(b) Drying state

Figure 6. Microscopic behaviour during the wetting and drying.

Figure 7 shows the depth of the CAC convection zone in the tidal and salt spray zones at the different erosion times. It can be seen that, after 30 d of erosion, all the CAC exhibited a clear chloride convection zone. Under an increase in the erosion time, the depth of the CAC convection zone in each group increased. In addition, the depth of the CAC convection zone in the tidal zone was lower than that in the salt spray zone. After erosion periods of 30, 60, 90, 120, and 180 d, the average depths of the convection zone in the tidal zone were 22.9 %, 25.0 %, 33.3 %, 26.3 %, and 21.1 % lower than those in the salt spray zone, respectively. This may be because the drying and wetting rate of the CAC in the salt spray zone was faster than that in the tidal zone; hence, the convection area further migrated to the interior of the concrete.

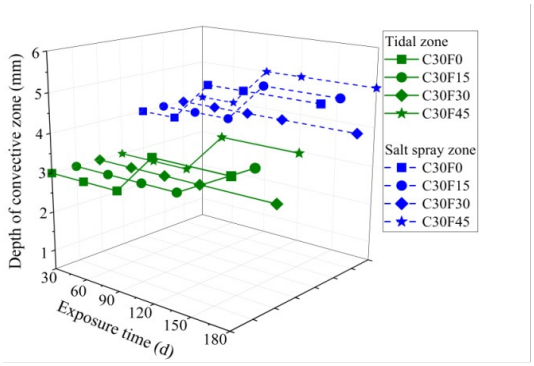

Figure 7. Depth of convection zone.

Influence of the erosion zone on the chloride diffusion

Figure 8 shows a comparison of the chloride concentration distribution of C30F15 at the different erosion zones. No convection zone was observed inside the concrete in the submerged zone; however, in the early stages of erosion, a convection zone was formed inside the concrete in the tidal and salt spray zones, though the locations of the convection zones differed. Compared with the tidal zone, the chloride saturation was lower and the capillary effect was

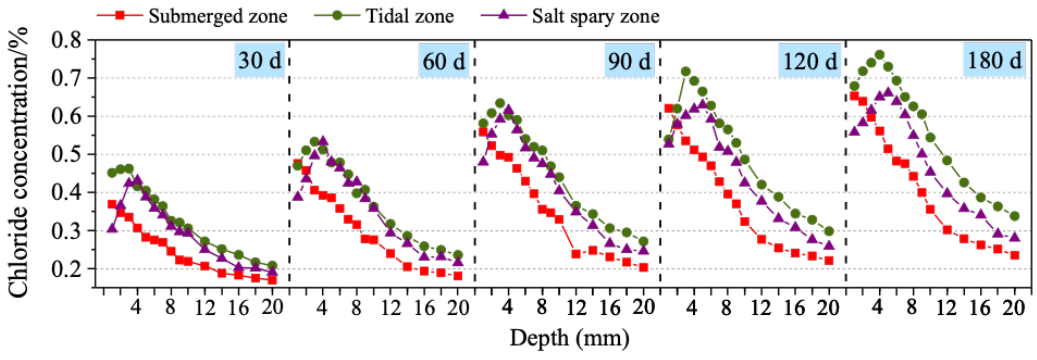

Figure 8. Comparison of the chloride concentration distribution of C30F15 under the different erosion zones.

more notable in the salt spray zone; hence, the depth of the convection zone shifted inward. Through comparison, it can be seen that, when the erosion time was within 90 days, the peak chloride concentration in the submerged zone was significantly lower than that in the tidal and salt spray zones at the same erosion time. When the erosion time exceeded 90 days, the peak chloride concentration in the submerged zone gradually approached that of the salt spray one. In addition, in the diffusion area at the peak chloride concentration and identical erosion depth, the chloride concentration value was tidal zone > salt spray zone > submerged zone, and the depth at which the chloride concentration stabilised was also deeper. Therefore, in the presence of the capillary adsorption and transport, the ingress depth of the chloride to concrete increased, and the time required for the chloride to reach the surface of the reinforcement became shorter, which had an adverse effect on the reinforced concrete structure.

Chloride diffusion coefficient

Figure 9 shows the variation in the chloride diffusion coefficient under the different erosion zones. The chloride diffusion coefficient of each concrete group gradually decreased with an increase in the erosion time. However, the chloride diffusion coefficient of the concrete exhibited marked differences. The chloride diffusion coefficient was the highest in the tidal zone, followed by the salt spray zone, while it was lowest in the submerged zone. The chloride diffusion coefficient decreased first and then increased with an increase in the FA content, and the differences between the different erosion zones were the smallest when the FA content was 30 %. At the initial stage of erosion, the chloride diffusion coefficient of the CAC in the submerged zone was lower than that in the salt spray zone; however, after 120 days of erosion, that in the submerged zone became slightly higher than that in the salt spray zone. In the submerged zone, the saturation of CAC was high, the migration of the chloride in the concrete was mainly achieved via diffusion, and the concentration difference inside and outside the concrete represented the main driving force. In the tidal and salt spray zones, the water saturation of the concrete was low, and the chloride was mainly transmitted to the concrete interior through capillary adsorption, which accelerated the ingress of chloride ions. In the tidal zone, after the dry concrete was placed into the erosion solution, the chloride ions migrated to the interior of the concrete under the joint action of capillary adsorption and diffusion. When the concrete was removed from the soaking solution and placed in a dry environment, the rapid evaporation of the pore liquid of the surface concrete caused the concentration of the salt solution to increase. When saturation was exceeded, the salt crystals precipitated and accumulated repeatedly to a certain extent, which damaged the concrete (i.e., produced new microcracks and further diffusion channels) and was conducive to the ingress of chloride.

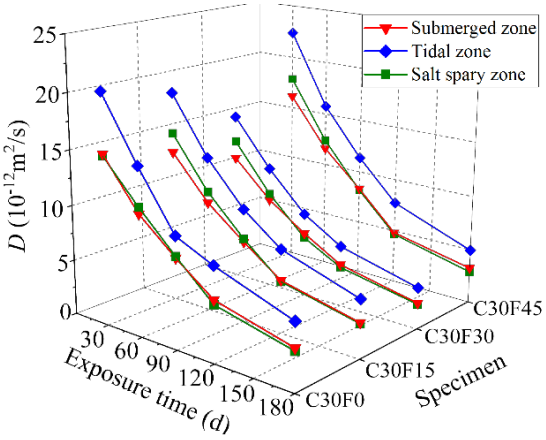

Figure 9. Chloride diffusion coefficient under the different erosion zones.

The above results show that the chloride diffusion coefficient follows a power function with respect to erosion time; this can be expressed as:

$$D(t) = D_0 \left(\frac{t_0}{t} \right)^m \quad (2)$$

where $D(t)$ is the chloride diffusion coefficient of the concrete at the erosion time t (10–12 $m^2 \cdot s^{-1}$), t_0 is the reference time of the diffusion coefficient(d), D_0 is the chloride diffusion coefficient at the reference time t_0 (10–12 $m^2 \cdot s^{-1}$), t is the erosion time (d), and m is the time attenuation coefficient of the chloride diffusion coefficient.

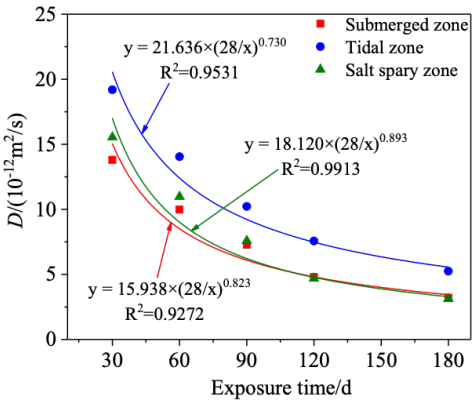

Figure 10. Fitting curves of the chloride diffusion coefficient attenuation.

By fitting the chloride diffusion coefficient of C30F15 exposed to the different erosion zones [using Equation 2], the time attenuation coefficient m of the concrete can be calculated; the fitting results are shown

in Figure 10. The correlation coefficients of the fitting results all exceeded 0.9. Therefore, the time attenuation coefficients of each group exposed to the different erosion zones were calculated [23]. Figure 11 shows the time attenuation coefficients of the CAC under the different erosion zones. The time attenuation coefficient of the CAC also followed the same change trend as the change in the erosion zone; that is, the sizes of the *m* values were salt spray zone > submerged zone > tidal zone, in which the m value under the salt spray zone was 10.8–28.5 % higher than that under the tidal zone, indicating that the chloride diffusion coefficient decreased fastest with respect to the increase in the erosion time under the salt spray zone. For the same erosion time, the time attenuation coefficient in the tidal zone was always smallest, and the damage to the concrete structure in the tidal zone was also the most serious. In addition, the time attenuation coefficient m increased under an increase in the FA content. The higher the FA content, the greater the time attenuation coefficient, and the faster the diffusion coefficient decreased under an increase in the erosion time.

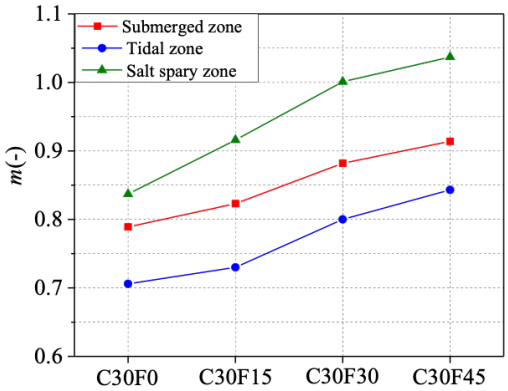

Figure 11. Time attenuation coefficient at the different erosion zones.

Microscopic analysis

XRD analysis

Figure 12 shows the XRD patterns for C30F15 in the different erosion zones after 90 d of erosion. The C30F15 concrete exhibited a clear Friedel's salt diffraction peak in the different erosion zones [24]. The intensity of Friedel's salt diffraction peak was the smallest in the submerged zone; meanwhile, no obvious differences were observed between the tidal and salt spray zones. This is because, at the initial stage of erosion, numerous chloride ions entered the concrete via the convection zone and reacted with the hydrated aluminium phase in the concrete to form Friedel's salt, producing a high Friedel salt content in the tidal and salt spray zones. The $Ca(OH)_2$ diffraction peak appeared at ~18°, the intensity of the $Ca(OH)_2$ diffraction peak was the highest in the submerged area, and the intensity of the $Ca(OH)_2$ diffraction peak was essentially the same as in the tidal and salt spray zones.

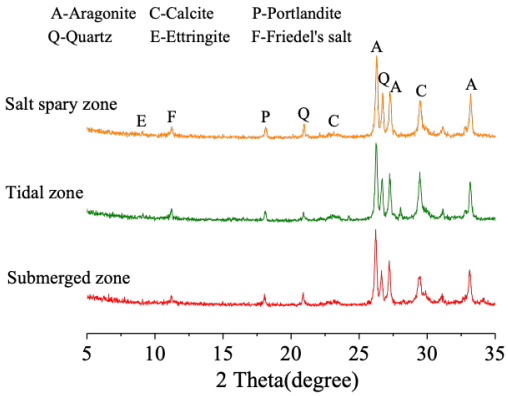

Figure 12. XRD patterns of C30F15 under the different erosion zones after 90 d of erosion.

TGA analysis

Figure 13 shows the derivative thermogravimetric (DTG) curves of the C30F15 concrete at 90 and 180 d of erosion under the different erosion zones. As shown in Figure 13(a), the endothermic peak area of Friedel's

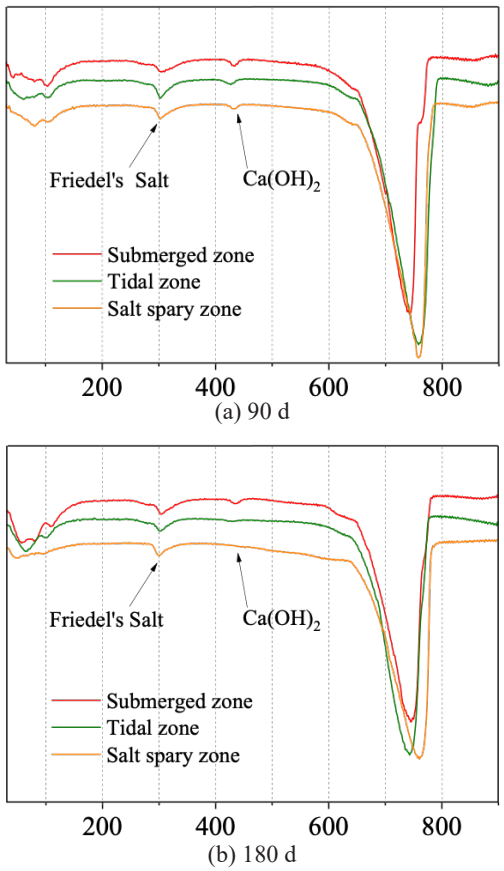

Figure 13. The DTG curves of C30F15 under the different erosion zones.

salt in the tidal and salt spray zones was significantly higher than that in the submerged zone at 90 d of erosion, which is consistent with the XRD test results. The convection action in the tidal and salt spray zones accelerated the ingress speed of the chloride ions, and more chloride ions diffused into the concrete at the same erosion time. Moreover, due to the convection action, the $Ca(OH)_2$ in the concrete was dissolved, lowering the alkalinity of the concrete. In Figure 13a, the area of the endothermal peak of $Ca(OH)_2$ in the tidal and salt spray zones was significantly smaller than that in the submerged zone. As shown in Figure 13b, after 180 d of erosion, an endothermic peak of $Ca(OH)_2$ appeared in the submerged zone, whereas no such peak appeared in the tidal and salt spray zones, indicating that presence of the convective zone in the tidal and salt spray zones would accelerate the dissolution of $Ca(OH)_2$. Moreover, when C_3S and C_2S were completely hydrolysed, the small content of $Ca(OH)_2$ meant that the C-S-H gel in the concrete was unstable, and decalcification occurred. In addition, with an increase in the erosion time, the area of the endothermic peak of Friedel's salt decreased in the tidal and salt spray zones; this was because, on the one hand, the physical adsorption capacity of the concrete decreased due to a decrease in the C-S-H, and, on the other hand, the liquid phase alkalinity of the concrete decreased owing to the dissolution of $Ca(OH)_2$, which promoted the decomposition of Friedel's salt.

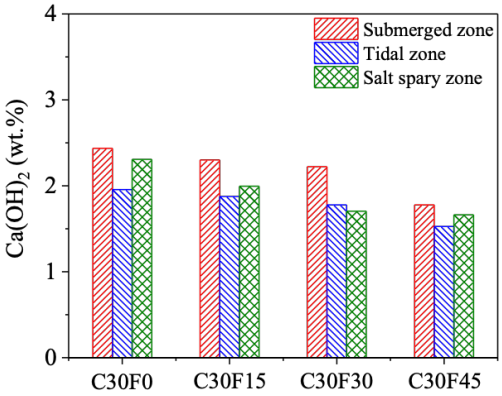

Figure 14. The content of $Ca(OH)_2$ in the CAC with the different erosion zones (90 d).

According to the TG results, the $Ca(OH)_2$ content in the CAC can be calculated according to the mass loss in the range of 410–470 °C [25]. Therefore, the $Ca(OH)_2$ content in the CAC in the different erosion zones after 90 d of erosion was calculated according to the thermogravimetric curve, as shown in Figure 14. It can be seen that the $Ca(OH)_2$ content of the CAC in the submerged zone exceeded that in the tidal and salt spray zones. With an increase in the FA content, the $Ca(OH)_2$ content in the CAC gradually decreased.

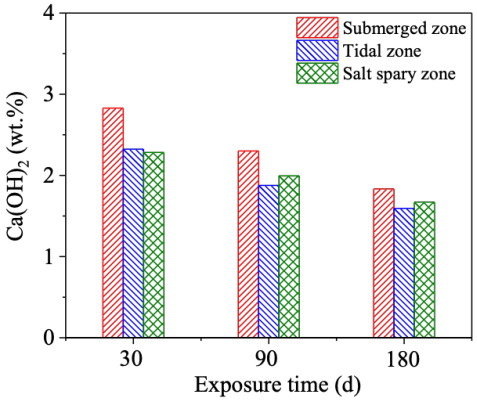

Figure 15. The content of $Ca(OH)_2$ in C30F15 with the different erosion time.

In the submerged, tidal and salt spray zones, the $Ca(OH)_2$ contents in C30F0 were 36.9 %, 28.1 % and 38.7 % higher than those in C30F45, respectively. Figure 15 shows the variation law of the $Ca(OH)_2$ content in C30F15 with respect to the erosion time. With an increasing erosion time, the $Ca(OH)_2$ content gradually decreased, and the difference between the different erosion zones also gradually decreased. At 180 d of erosion, the $Ca(OH)_2$ contents in the submerged, tidal and salt spray zones decreased by 22.9 %, 29.5 % and 32.1 %, respectively, compared with those at 30 d of erosion.

CONCLUSIONS

1. In the submerged zone, the chloride concentration in the CAC decreased under an increasing erosion time. In the tidal and salt spray zones, the chloride concentration exhibited a two-stage distribution pattern with ascending and descending phases forming a peak chloride concentration in the concrete. At identical erosion times, the peak chloride concentration in the tidal zone exceeded that in the salt spray zone.
2. In the early stage of erosion, a clear convective zone appeared in the tidal and salt spray zones, and the depths of the convective zone in the tidal and salt spray zones were 3–4 and 4–5 mm, respectively; furthermore, the depth of the convective zone increased with an increasing erosion time.
3. The chloride diffusion coefficient of the CAC exhibited a power function attenuation law under an increase in the erosion time. Across all the erosion times, the chloride diffusion coefficient was the largest in the tidal zone, followed by the salt spray zone, while it was the smallest in the submerged zone. The attenuation coefficient of the chloride diffusion coefficient increased with an increase in the FA content, and the value under the salt spray zone was 10.8–28.5 % larger than that in the tidal zone.
4. The $Ca(OH)_2$ content of the CAC in the submerged zone was greater than that in the tidal and salt spray

zones. With an increase in the erosion time, the $Ca(OH)_2$ content gradually decreased, and the difference between the different erosion zones likewise gradually decreased.

Acknowledgment

This study is financially supported by the National Natural Science Foundation of China (No. 51590914).

REFERENCES

1. Chai Y., Niu Y., Li, W., Lv H. (2021): Research progress on improved technology of coral aggregate concrete. *Materials Reports, 35*(15), 15134-15142.
2. Su L., Niu D., Luo Y., Huang D., Luo D. (2021): Inner chloride ion diffusion and capillary water absorption properties of fly ash coral aggregate concrete. *Journal of Building Materials, 24*(1),77-92.
3. Liu J., Ou Z., Peng W., Guo T., Deng W., Chen Y. (2017): Literature review of coral concrete. *Arabian Journal for Science and Engineering, 43*(4), 1-13. doi: 10.1007/s13369-017-2705-x
4. Chu Y., Wang A., Zhu Y., Wang H., Liu K., Ma R., Guo L., Sun D. (2021): Enhancing the performance of basic magnesium sulfate cement-based coral aggregate concrete through gradient composite design technology. *Composites Part B: Engineering, 227*, 109382. doi: 10.1016/j.compositesb.2021.109382
5. Zhou L., Guo S., Zhang Z., Shi C., Jin Z., Zhu D. (2021): Mechanical behavior and durability of coral aggregate concrete and bonding performance with fiber-reinforced polymer (FRP) bars: A critical review. *Journal of Cleaner Production, 289*,125652. doi: 10.1016/j.jclepro.2020.125652
6. Su L., Niu D., Luo D. (2018): Research of coral aggregate concrete on mechanical property and durability. *Materials Reports, 32* (10), 3387-3393.
7. Yu H., Da B., Ma H., Zhu H., Yu Q., Ye H. (2017): Durability of concrete structures in tropical atoll environment. *Ocean Engineering, 135*, 1-10. doi: 10.1016/j.oceaneng.2017.02.020
8. Guo D., Su C., Peng Z., Li Q., Chen W. (2018): Mechanical properties and microstructure of concrete prepared with coral reef sand and sea water. *Journal of Building Materials, 21*(1), 41-46.
9. Huang D., Niu D., Su L., Fu Q. (2021): Chloride diffusion behavior of coral aggregate concrete under drying-wetting cycles. *Construction and Building Materials, 270*, 121485. doi: 10.1016/j.conbuildmat.2020.121485
10. Liang X., Yin S., Hu C. (2021): Environmental reduction factors of BFRP bars in coral aggregate concrete in high temperature and high humidity environments. *Structures, 33*, 3017-3024. doi: 10.1016/j.istruc.2021.06.021
11. Huang D., Niu D., Su L., Liu Y., Guo B., Xia Q., Peng G. (2022): Diffusion behavior of chloride in coral aggregate concrete in marine salt-spray environment. *Construction and Building Materials, 316*, 125878. doi: 10.1016/j.conbuildmat.2021.125878
12. Wattanachai P., Otsuki N., Saito T., Nishida T. (2009): A Study on Chloride Ion Diffusivity of Porous Aggregate Concretes and Improvement Method. *Doboku Gakkai Ronbunshuu E, 65* (1),30–44. doi: 10.2208/jsceje.65.30
13. Da B., Yu H., Ma H., Zhang Y., Dou X. (2016): Surface free chloride concentration and apparent chloride diffusion coefficient of coral seawater concrete. *Journal of Southeast University, 46*(5), 1093-1097.
14. Dou X., Yu H., Ma H., Da B., Yuan Y., Mi R. (2016): Surface chloride concentration of coral concrete exposed to marine environment. *Bulletin of The Chinese Ceramic Society, 35* (9), 2695-2700.
15. Huang D., Niu D.,Zheng H., Su L., Luo D., Fu Q. (2020): Study on Chloride Transport Performance of Eco-Friendly Coral Aggregate concrete in marine Environment. *Construction and Building Materials, 258*, 120272. doi: 10.1016/j.conbuildmat.2020.120272
16. He H. (2009): Analysis and quantification of carbon dioxide emission from cement production. *Cement Engineering, 1*, 61-65.
17. Liu R., Durham S.A., Rens K.L. (2011): Effects of post-mercury-control fly ash on fresh and hardened concrete properties. *Construction and Building Materials, 25*(8), 3283-3290. doi: 10.1016/j.conbuildmat.2011.03.016
18. Wang Y., Li Z., Qin Y., Wang W. (2018): Effect of replacement of recycled coarse aggregate on compressive strength of concrete. *Concrete, 12*,27-30.
19. Cheng S., Shui Z., Sun T.; Yu R.; Zhang G., Ding S. (2017): Effects of fly ash, blast furnace slag and metakaolin on mechanical properties and durability of coral sand concrete. *Applied Clay Science, 141*, 111-117. doi: 10.1016/j.clay.2017.02.026
20. Zhang Z., Sang Z., Zhang L., Yu R.; Ma Z.,Zhang Y. (2013): Experimental research on durability of concrete made by seawater and sea-sand. *Advanced Materials Research, 641*, 385-388. doi: 10.4028/www.scientific.net/AMR.641-642.385
21. Babaee M., Castel A. (2016): Chloride-induced corrosion of reinforcement in low-calcium fly ash-based geopolymer concrete. *Cement and Concrete Research, 88*, 96-107. doi: 10.1016/j.cemconres.2016.05.012
22. Li C. (2009). *Study on water and lonic transport processes in cover concrete under drying-wetting cycles*. PhD Dissertation, Tsinghua University.
23. Thomas M.D.A., Matthews J.D. (2004): Performance of pfa concrete in a marine environment-10-year results. *Cement and Concrete Composites, 26* (1), 5-20. doi: 10.1016/S0958-9465(02)00117-8
24. Yue Y., Wang J, Basheer P.A.M., Bai Y. (2018): Raman spectroscopic investigation of Friedel's salt. *Cement and Concrete Composites, 86*, 306–314. doi: 10.1016/j.cemconcomp.2017.11.023
25. Huang D., Niu D., Su L., Pan D., Liu Y. (2022): Durability of coral aggregate concrete under coupling action of sulfate, chloride and drying-wetting cycles. *Case Studies in Construction Materials, 16*, e01003. doi: 10.1016/j.cscm.2022.e01003